Journal of Biomolecular NMR, **22:** 89–92, 2002.
KLUWER/ESCOM

Letter to the Editor: The NMR structure of the class I human ubiquitin-conjugating enzyme 2b

Takaaki Miura[a,b,*], Werner Klaus[a,*], Alfred Ross[a], Peter Güntert[c] & Hans Senn[a]
[a]*Department of Chemical Techonologies, F. Hoffmann-La Roche AG, CH-4070 Basel, Switzerland;* [b]*Nippon Roche Research Center, Kamakura, Kanagawa, 247-8530 Japan;* [c]*Institut für Molekularbiologie & Biophysik, Eidgenössische Technische Hochschule, Hönggerberg, CH-8093 Zürich, Switzerland*

Received 24 September 2001; Accepted 1 November 2001

Key words: heteronuclear NMR, NMR structure, ubiquitin-conjugating enzyme

Abbreviations: E2 and Ubc – Ubiqutin-conjugating enzyme; HsUbc2b – Human ubiquitin-conjugating enzyme 2b.

Biological context

The covalent attachment of the polypeptide ubiquitin to cellular proteins, termed 'ubiquitination', plays a pivotal role in a variety of eukaryotic cellular events including cell-cycle progression, signal transduction, and transcriptional regulation (for a recent review, see Ciechanover et al., 2000). It constitutes an intracellular signal to mark protein-substrates for the degradation by the 26S proteasome. Ubiquitin conjugation proceeds via three enzymatic reactions. Initially, a high-energy thioester bond is formed between the C-terminal glycine of Ubiquitin and Ubiquitin-activating enzyme (E1 or Uba) in an ATP-dependent manner. In a next step, ubiquitin is transferred to a ubiquitin-conjugating enzyme (E2 or Ubc), maintaining the thioester bond. This reaction is followed by the covalent attachment of ubiquitin to the ε-amino group of one or more lysine residues of the target proteins mostly in conjunction with an ubiquitin-protein ligase (E3 or Ubr). The process of ubiquitination can be repeated by the attachment of another ubiquitin-molecule to the lysine residue of the conjugated ubiquitin to form a polyubiquitin chain, which is required for an efficient recognition by the 26S proteasome.

Ubc's represent a family of closely related proteins that vary in size from 14–35 kDa. A core catalytic domain of approximately 150 residues which include a ubiquitin-accepting cysteine is relatively conserved. Human ubiquitin-conjugating enzyme 2b (HsUbc2b, 152 amino acids, also known as E2-14K), together with its cognate RING-containing E3 enzyme E3α, is involved in the so-called N-end rule pathway (Sung et al, 1991). The mRNA level of E2-14k has been reported to be up-regulated during increased muscle proteolysis in tumor-bearing cachectic rat models (Temparis et al., 1994). Furthermore, it has been shown that the enhanced proteolysis in this model was not due to the other major proteolytic pathways. These lines of evidence suggest that HsUbc2b provides an attractive target for the development of a new class of anticachexia drugs. The first step of the structure-based drug design is to obtain a high-resolution tertiary structure of the target protein. Here, we describe the NMR structure of HsUbc2b.

Methods and results

Sample preparation, NMR measurements, processing of spectra and sequential assignment of the backbone signals as well as C^{β} and H^{β} signals of the HsUbc2b have been done as reported previously (Miura et al., 1999).

All non-exchangeable side chain ^{1}H, ^{15}N and ^{13}C resonances except for some atoms of the side chains of Lys, Arg and Pro were assigned by the combined analyses of various 2D, 3D and 4D homonuclear and heteronuclear spectra which include 2D homonuclear-TOCSY and NOESY, 2D ^{1}H-TOCSY-relayed ct-[^{13}C, ^{1}H]-HMQC and ^{1}H-^{13}C HMQC optimized for the aromatic region (Zerbe et al., 1996), 3D C_DIP(CO)NH, 3D H_DIP(CO)NH (Grzesiek et al., 1993), 4D-^{15}N/^{13}C-NOESY-HMQC-HSQC,

*To whom correspondence should be addressed. E-mails: takaaki.miura.tm2@roche.com; werner.klaus.wk1@roche.com

Table 1. Summary of statistics for the 20 final structures

NOE upper distance limits	1475	
Intra-residual	441	
Sequential	332	
Medium-range	204	
Long-range	498	
Dihedral angle constraints	286	
Hydrogen bonds	2 × 70	
Residual DYANA target function, Å^2	1.36 ±	0.36
Residual NOE violations		
Number > 0.1 Å	19 ±	6
Maximum, Å	0.14 ±	0.05
Residual angle violations		
Number > 2.0°	1 ±	1
Maximum, °	2.55 ±	0.75
Amber energies, kcal mol^{-1}		
Total	−5515 ± 139	
van der Waals	−513 ± 13	
Electrostatic	−6197 ± 132	

Atomic rmsd values (Å)	Backbone atoms	All heavy atoms
Residues 4–148	0.69	1.39
α-Helices and β-strands	0.61	1.44

Ramachandran plot (%)	
Most favorable region	90.6
Allowed region	9.1
Disallowed region	0.3

Helices: Pro4-Gln18, Val102-Asp114, Asn124-Gln131, Lys134-Ser148.
Strands: Val24-Pro28, Glu35-Phe41, Thr52-Glu58, Thr69-Phe72.

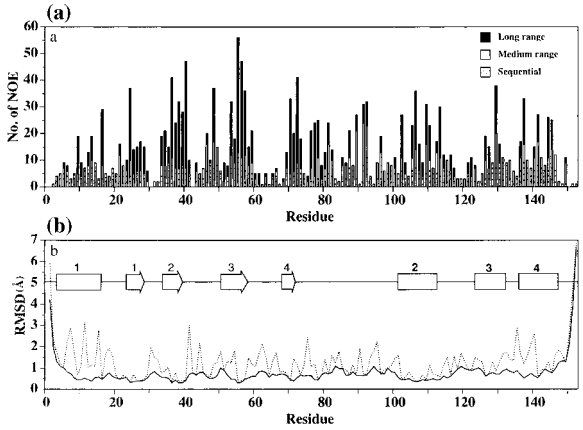

Figure 1. (a) Number and distribution of NOE-derived distance constraints along the sequence of HsUbc2b: sequential (hatched bars), medium-range (open bars), long-range (filled bars). (b) Plot of RMSD-values of backbone (continuous line) and side-chain (dotted line) heavy atoms after global superposition of the final 20 structures for minimum deviation. The location of the secondary structure elements is also shown in the upper part.

3D-HCCH-TOCSY, 3D-^{13}C-NOESY, 4D-^{13}C, ^{13}C-NOESY-HSQC-HSQC. Stereospecific assignments of the methyl groups of all Val and Leu were made by recording a ^{1}H-^{13}C CT-HSQC spectrum for fractionally ^{13}C labeled HsUbc2b according to Hiroaki et al. (1997). Stereospecific assignments for 74 non-degenerate diastereotopic groups were identified by comparison of upper distance limits with a preliminary structure. Of 14 proline residues occurring in the sequence of HsUbc2b, only Pro64 is found in a *cis*-conformation as evidenced by the observation of NOEs between the α-protons of Tyr63 and Pro64.

The determination of the three-dimensional structure of HsUbc2b was performed with the automated NOE assignment module CANDID (T. Herrmann, P. Güntert and K. Wüthrich, unpublished) in the program DYANA (Güntert et al., 1997). CANDID/DYANA performs automated assignment and distance calibration of NOE intensities, removal of meaningless distance constraints, structure calculation with torsion angle dynamics, and automatic NOE upper distance limit violation analysis. Tables of assigned NMR chemical shifts and unassigned NOESY cross peaks derived from four multi-dimensional NOESY spectra (2D homonuclear NOESY (100 ms mixing time), 3D ^{15}N NOESY-HSQC (40 ms), 3D ^{13}C NOESY-HSQC (80 ms), and 4D-^{13}C, ^{13}C-NOESY-HSQC (80 ms)) were provided as input to CANDID/DYANA, and the resulting NOE cross peak assignments were subsequently confirmed by visual inspection of the spectra. The CANDID/DYANA calculation consisted of seven cycles of iterative NOE assignment and structure calculation. In each cycle NOE assignments were generated by the program on the basis of the agreement between peak positions and chemical shift values, the consistency with the assignments of other NOEs ('network-anchored assignment'), and, from cycle two onwards, the agreement with the structure from the preceding cycle. During the first six CANDID cycles, ambiguous distance constraints (Nilges et al., 1997) were used to introduce the information from the NOE cross peaks that are not (yet) unambiguously assigned into the structure calculation. This was especially important at the outset of the calculation because less than 5% of the NOEs could be assigned unambiguously on the basis of chemical shift information alone. For the last cycle of the CANDID/DYANA calculation, however, only distance constraints were retained

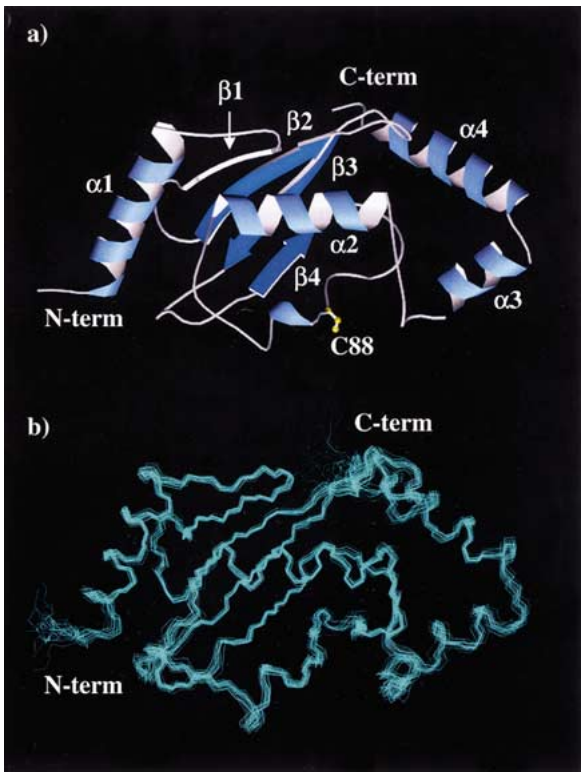

Figure 2. (a) Ribbon representation of the NMR solution structure of HsUbc2b. The location of helices and strands is indicated in white together with the side chain of the active site Cys88 shown as a ball and stick representation. (b) Superposition of the ensemble of the final 20 energy-minimized DYANA structures of HsUbc2b. The structures are superimposed for minimum mutual deviation of the backbone atoms (N, C^{α}, C', O) from Ala5 to Trp147.

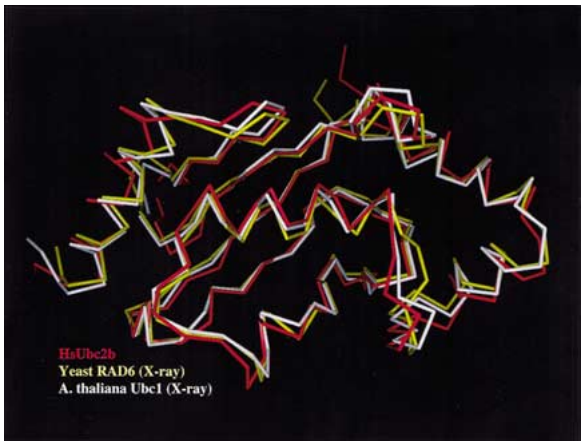

Figure 3. Superposition of the C_{α} backbone representation of the NMR structure of HsUbc2b with two X-ray structures of HsUbc2b homologues, *A. thaliana* Ubc1 (Cook et al., 1992) and *S. cerevisiae* RAD6 (Worthylake et al., 1998). The HsUbc2b structure is shown in red, Ubc1 in white, RAD6 in yellow.

that corresponded to unambiguously assigned NOE cross peaks. NOE intensities were converted with the program DYANA into upper distance bounds according to an inverse sixth power peak volume-to-distance relationship (Güntert et al., 1991).

The final structure calculation was based on 1475 meaningful distance constraints derived from 2953 unambiguously assigned NOESY cross peaks. The number of NOE constraints for each residue is shown in Figure 1a. Within regular secondary structure elements delineated by NOEs, hydrogen bonds were deduced from NH exchange experiments, and two distance constraints, $r_{NH\text{-}O}$ = 1.5–2.8 Å and $r_{N\text{-}O}$ = 2.4–3.5 Å, were applied for each hydrogen bond. Dihedral angle constraints for backbone ϕ,ψ angles were generated by the combined information from NOE patterns, $^{13}C^{\alpha}$ and $^{1}H^{\alpha}$ secondary chemical shifts, and the $^{3}J^{HNH\alpha}$ coupling constants derived from the 3D HNHA spectrum. In addition, those resulting from the program TALOS (Cornilescu et al., 1999), were added where appropriate. These were further supplemented with 13 χ^1 and 15 χ^2 constraints derived from $^{3}J^{C\gamma N}$ and $^{3}J^{C\gamma C'}$, and $^{3}J^{C\delta C\alpha}$ coupling constants which were measured for the methyl containing residues from the ^{13}C-{^{15}N} and ^{13}C-{$^{13}C'$}-spin-echo difference experiments (Vuister et al., 1993), and the 3D LRCC spectrum (Bax et al., 1992), respectively. Final structure calculations using the standard DYANA torsion angle dynamics protocol (Güntert et al., 1997) with 12 000 steps were started from 100 randomized conformers. The 20 structures with the lowest values of the DYANA target function were subjected to an energy-minimization in a water shell with the program OPALp (Koradi et al., 2000) using the AMBER force field (Cornell et al., 1995). Table 1 provides a statistical overview on the 20 conformers that represent the HsUbc2b NMR structure. The rms deviations for backbone (C', C^{α}, N, O) and side-chain heavy atoms for each residue are shown in Figure 1b, together with the location of the secondary structure elements as identified with the program MOLMOL (Koradi et al., 1996). Overall, the bundle of NMR-derived structures of HsUbc2b is well-defined with a backbone rmsd-value of 0.61 Å for residues located in helices and strands. In regions with a lower number of restraints the variation among the conformations is larger amounting to rmsd-values of about 1 Å for residues Ala83-Gly85, Asn94, Pro98 and for the loop-segment Pro118-Ser124 (Figure 1b and Figure 2b).

Figure 2a provides a schematic representation of the NMR structure of HsUbc2b. The conformation is that of a single-domain α/β protein comprising a four-stranded antiparallel β-sheet (Val24-Pro28, Glu35-Phe41, Thr52-Glu58, Thr69-Phe72) and four α-helices (Pro4-Gln18, Val102-Asp114, Asn124-Gln131, Lys134-Ser148). With one side the sheet is twisted around the second α-helix while its other face is exposed to the solvent. The first α-helix packs against one end of the sheet, the third and fourth helices flank the other end. The active site Cys88 is located in the middle of a segment that connects the fourth strand with the second helix. This part also contains a short 3_{10} helix (Asp90-Leu92) which is followed by a solvent-exposed loop that leads into the second α-helix. Another surface loop is found between the second and third helix. Both loops together form a shallow cleft above the active site Cys88.

Discussion and conclusions

The NMR-conformation of HsUbc2b agrees closely with the published X ray structures of eight proteins containing a *Ubc* domain. Two of them, Rad6 from *S. cerevisiae* (Worthylake et al., 1998) and Ubc1 from *A. thaliana* (Cook et al., 1992), fall into the same family of E2's as HsUbc2b, sharing 63% and 75% of their amino acid sequences with HsUbc2b, respectively. There is no amino acid insertion in the *Ubc* domain part of these three proteins. An overlay of the averaged NMR structure obtained from the final ensemble of HsUbc2b with the structure of each of these two proteins shows that there is no significant difference in the overall topology (Figure 3). The rms differences for the C^{α} atoms of residues 5–147 are 1.26 Å and 1.45 Å for Rad6 and plant Ubc1, respectively. The largest deviations occur in the region between Asn115 and Pro121, the second surface loop close to the active site Cys88. Based on smaller heteronuclear NOE values, as observed by NMR for this region, it has been shown that this segment is flexible on a nanosecond to picosecond time scale (Miura et al., 1999). In the crystal structure of Rad6 with three protein molecules in the asymmetric unit a large displacement of this loop by up to 3.9 Å for Pro118 is found for one of them (Worthylake et al., 1998). Because these alternate loop conformations affect the exposure of the active site cysteine these authors consider it possible that this mobility is necessary for the function of Ubc.

The ^{1}H, ^{15}N, and ^{13}C assignments and the atom coordinates have been deposited in the BioMagResBank (accession code BMRB-5038) and in the Protein Data Bank (PDB ID code 1jas), respectively.

Acknowledgement

We thank Torsten Herrmann for help with the CANDID calculations.

References

Bax, A., Max, D. and Zax, D. (1992) *J. Am. Chem. Soc.*, **114**, 6923–6925.

Ciechanover, A., Orian, A., and Schwartz, A.L. (2000) *BioEssays*, **22**, 442–451.

Cook, W.J., Jeffrey, L.C., Sullivan, M.L. and Vierstra, R.D. (1992) *J. Biol. Chem.*, **267**, 15116–15121.

Cornell, W.D., Cieplak, P., Bayly, C.I., Gould, I.R., Merz Jr., K.M., Ferguson, D.M., Spellmeyer, D.C., Fox, T., Caldwell, J.W. and Kollman, P.A. (1995) *J. Am. Chem. Soc.*, **117**, 5179¡5197.

Cornilescu, G., Delaglio, F. and Bax, A. (1999) *J. Biomol NMR*, **13**, 289–302.

Grzesiek, S., Anglister, J. and Bax, A. (1993) *J. Magn. Reson.*, **B101**, 114–119.

Güntert, P., Braun, W. and Wüthrich, K. (1991) *J. Mol. Biol.*, **217**, 517–530.

Güntert, P., Mumenthaler, C. and Wüthrich, K. (1997) *J. Mol. Biol.*, **273**, 283–298.

Hiroaki, H., Klaus, W. and Senn, H. (1996) *J. Biomol. NMR*, **8**, 105–122.

Koradi, R., Billeter, M. and Güntert, P. (2000) *Comput. Phys. Commun.*, **124**, 139–147.

Koradi, R., Billeter, M. and Wüthrich, K. (1996) *J. Mol. Graph.*, **14**, 51–55

Miura, T., Klaus, W., Gsell, B., Miyamoto, C. and Senn, H. (1999) *J. Mol. Biol.*, **290**, 213–228.

Nilges, M., Macias, M.J., O'Donoghue, S.I. and Oschkinat, H. (1997) *J. Mol. Biol.*, **269**, 408–422.

Sung, P., Berleth, E., Pickart, C., Prakash, S. and Prakash, L. (1991) *EMBO J.*, **10**, 2187–2193.

Temparis, S., Asensi, M., Taillandier, D., Aurousseau, E., Larbaud, D., Obled, A., Bechet, D., Ferrara, M., Estrela, J.M. and Attaix, D. (1994) *Cancer Res.*, **54**, 5548–5573.

Vuister, G.W., Wang, A.C. and Bax, A. (1993) *J. Am. Chem. Soc.*, **115**, 5334–5335.

Worthylake, D.K., Prakash, S., Prakash, L. and Hill, C.P. (1998) *J. Biol. Chem.*, **273**, 6271–6276.

Zerbe, O., Szyperski, T., Ottiger, M. and Wüthrich, K. (1996) *J. Biomol. NMR*, **7**, 99–106.